



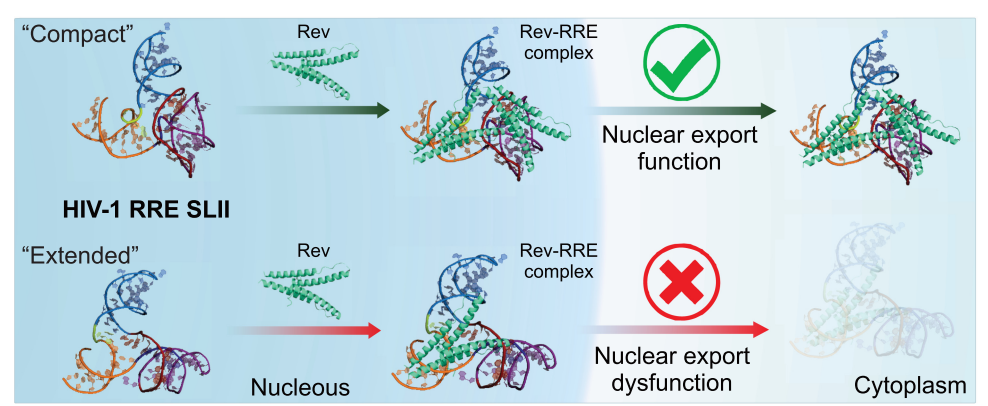
Mutation-driven RRE stem-loop II conformational change induces HIV-1 nuclear export dysfunction

Manju Ojha¹, Lucia Hudson¹, Amanda Photenhauer², Trinity Zang³, Lauren Lerew⁴, Şölen Ekesan ^{©4}, Jason Daniels¹, Megan Nguyen¹, Hardik Paudyal¹, Darrin M. York⁴, Melanie D. Ohi^{2,5}, Jan Marchant¹, Paul D. Bieniasz ^{©3}, Deepak Koirala ^{©1,*}

Abstract

The Rev response element (RRE) forms an oligomeric complex with the viral protein Rev to facilitate the nuclear export of intron-retaining viral RNAs during the late phase of HIV-1 (human immunodeficiency virus type 1) infection. However, the structures and mechanisms underlying this process remain largely unknown. Here, we determined the crystal structure of the HIV-1 RRE stem-loop II (SLII), revealing a unique three-way junction architecture in which the base stem (IIa) bifurcates into the stem-loops (IIb and IIc) to compose Rev binding sites. The crystal structures of various SLII mutants demonstrated that while some mutants retain the same "compact" fold as the wild type, other single-nucleotide mutants induce drastic conformational changes, forming an "extended" SLII structure. Through *in vitro* Rev binding assays and Rev activity measurements in HIV-1-infected cells using structure-guided SLII mutants designed to favor specific conformers, we showed that while the compact fold represents a functional SLII, the alternative extended conformation inhibits Rev binding and oligomerization and consequently stimulates HIV-1 RNA nuclear export dysfunction. The propensity of SLII to adopt multiple conformations as captured in crystal structures and their influence on Rev oligomerization illuminate emerging perspectives on RRE structural plasticity-based regulation of HIV-1 nuclear export and provide opportunities for developing anti-HIV drugs targeting specific RRE conformations.

Graphical abstract



Introduction

The human immunodeficiency virus type 1 (HIV-1) consists of about 9-kb-long genomic RNA that encodes the proteins required for virus proliferation in the host cells [1–3]. During infection, the proviral DNA integrated within the host genome produces a transcript that undergoes alternative splicing or re-

mains unspliced to yield intron-less or intron-retaining RNAs. These RNAs are eventually exported to the cytoplasm to be translated into viral proteins or packaged into new virions [1–3]. Because the host nuclear export machinery does not transport unspliced or intron-retaining RNAs, several retroviruses, including HIV-1, have evolved specific mechanisms

Department of Chemistry and Biochemistry, University of Maryland, Baltimore County, Baltimore, MD 21250, United States

²Life Sciences Institute, University of Michigan, Ann Arbor, MI 48109, United States

³Laboratory of Retrovirology, The Rockefeller University, New York, NY 10065, United States

⁴Department of Chemistry and Chemical Biology, Laboratory for Biomolecular Simulation Research, and Institute for Quantitative Biomedicine, Rutgers University, Piscataway, NJ 08854, United States

⁵Department of Cell and Developmental Biology, University of Michigan, Ann Arbor, MI 48109, United States

^{*}To whom correspondence should be addressed. Email: dkoirala@umbc.edu

to promote the nuclear export of such RNA species [4–6]. In HIV-1, a viral protein called Rev recognizes a unique *cis*-acting RNA structure called the Rev response element (RRE) found within the intronic regions of unspliced or partially spliced RNAs [5–9]. Such RRE–Rev assembly then interacts with the host machinery to guide the nuclear export of these viral RNAs through the Crm1 pathway [10–12]. As this RRE–Rev platform is essential for viral proliferation, it has been an attractive target for therapeutic interventions against HIV-1 infection [13–15]. However, the molecular mechanisms of RRE-mediated nuclear export of HIV-1 RNAs remain elusive, mainly due to the lack of high-resolution structures of the RRE and well-defined structural models for its interactions with Rev.

HIV-1 RRE comprises \sim 350 nucleotides [2, 7–9]. However, previous computational, enzymatic, and chemical probing experiments with mutant and truncated constructs have identified that \sim 232 nucleotides are sufficient to form the functional core of the RRE [16, 17]. The proposed secondary structure comprises five subdomains: I to V, with II to V being the stemloops (SLs) that branch out from base stem I (Fig. 1A), and SLII is known to form a three-way junction (3WJ) structure, where the base stem IIa bifurcates into stem loops IIb and IIc. Within this RRE secondary structural model, an asymmetric purine-rich bulge within the stem I and the 3WI region of SLII have been identified as the high-affinity binding sites for Rev [18-24]. While it is known that multiple Revs bind to the RRE to form a homo-oligomeric ribonucleoprotein (RNP) complex, how different structural features within the RRE orchestrate the binding of various Rev oligomers to construct a functional RRE-Rev complex remains unclear. For instance, significant alterations, such as the complete deletion of SLII, eliminate Rev binding and nuclear export activity, whereas disruption of SLs III and IV does not exhibit such a drastic effect [25–28].

Several studies have investigated the structures and interactions of HIV-1 RRE to illuminate the possible mechanism of RRE structure-mediated nuclear export of HIV-1 RNA species. Phylogenetic and biochemical probing studies have provided secondary structure information on HIV-1 RRE, including base pairings and nucleotide accessibility [20, 24, 29– 31]. Results from these studies led to a model where the fulllength HIV-1 RRE can adopt multiple conformations, with the five- and four-stem-loop conformations being the most prevalent forms [24, 31, 32]. Conformational diversity has been shown to originate due to the structural rearrangements of SLs III and IV; however, secondary structures of SLII, the highaffinity Rev binding site, remained virtually unchanged in those models [2, 24, 30–32]. Therefore, SLII has been the focus of several biochemical and structural studies to understand the nature of RRE-Rev interactions and the RRE-mediated HIV-RNA nuclear export mechanism. Nuclear magnetic resonance (NMR) and X-ray crystallographic studies of isolated IIb constructs alone and in complex with a Rev peptide not only illuminated how Rev binds to the RNA through base-specific hydrogen bonds and electrostatic interactions with the phosphodiester backbone but also underscored that this RNA likely undergoes some conformational changes upon Rev binding [33–38], indicating a structurally plastic nature of the RNA. Such plasticity at the SLII 3WJ seemed necessary for the effective binding of multiple Rev molecules [21–23, 35, 38], a model further supported by a crystal structure of the isolated

IIb construct with an engineered junction site in a complex with the Rev dimer [37]. It is also consistent with high SHAPE reactivities observed for the IIb near the 3WI nucleotides in the context of the intact RRE sequence, which agrees with the highly flexible nature of the Rev binding sites [2, 31, 32]. These observations with the isolated IIb structures indicate the possibility of similar conformational flexibility for the intact SLII 3WJ, possibly modulating the Rev binding to the HIV-1 RRE. However, other than structures of select SLII fragments [33–38], a small-angle X-ray scattering (SAXS)-based study proposing a low-resolution model with an unusual Ashaped topology for an intact HIV-1 RRE [39] and a recently reported SLII crystal structure [40], the nature of RRE structural plasticity and how it modulates Rev interactions, and the mechanism of HIV-1 RNA nuclear export remain largely unknown.

Here, we report the high-resolution crystal structure of intact SLII folded in a different conformation than the previously reported crystal structure with a transfer RNA (tRNA) scaffold [40]. We also crystallized four structure-guided SLII mutants and revealed that while some mutant structures retained the same fold as the wild-type structure, other singlenucleotide mutations induced drastic conformational changes. One of the SLII conformers exhibits extensive interactions between the 3WI junction-forming nucleotides with a tight arrangement of the stems around the 3WI, designated as the "compact" form. The second SLII conformer folds into a more open arrangement and elongated IIb, termed the "extended" form. Although both conformers may coexist in solution, our findings from combined negative-stain electron microscopy (EM), molecular dynamics (MD) analysis, and biochemical Rev binding assays show that, while the extended conformation seems thermodynamically favored in solution, the compact conformation of SLII, stabilized by engineered mutations, supports more robust Rev binding and oligomerization compared to the extended form. Furthermore, the compact form is consistent with a Rev-bound conformation in vivo that promotes nuclear export, as indicated by Rev activity measurements in HIV-1-transfected human cells. Notably, our compact and extended folds crystallized in separate crystals differ significantly from those designated as "closed" and "open" conformations reported by Tipo et al. [40], which were observed within crystallographic asymmetric units of the same crystal. While Rev may prefer to bind a sampled RRE conformation or induce binding-favorable conformational alterations within the RRE structure in cells, our findings, combined with earlier structural results, suggest a model where the plasticity of the SLII could act as a structural regulator to modulate Rev binding and oligomerization to the HIV-1 RRE, shedding light on the Rev-RRE-mediated HIV-1 nuclear RNA export mechanism and providing unique opportunities to develop RRE conformation-specific anti-HIV therapeutics.

Materials and methods

Materials

The sequences of the RRE SLII constructs used in this study are listed in Supplementary Table S1. Unless stated otherwise, all single-stranded DNA templates and polymerase chain reaction (PCR) primers for these constructs were purchased from Integrated DNA Technologies (IDT) Inc.

RNA synthesis and purification

The RNA constructs were synthesized by *in vitro* transcription and purified by denaturing polyacrylamide gel electrophoresis, as described elsewhere [41, 42]. See the supporting information for further details.

Rev expression and purification

The HIV-1 Rev gene was cloned into a pET19b vector (Gen-Script) with a 6xHis tag at the N-terminal and MBP tag, and the plasmid containing this MBP tag-fused Rev was transformed into BL21 (DE3) Escherichia coli. The bacterial culture was grown in LB supplemented with 100 µg/ml of ampicillin at 37° C with 250 rpm in a 5 ml starter culture for \sim 12 h (overnight), which was then used to inoculate a 1 litre culture for overnight growth (until the OD of ~ 0.6). The protein overexpression was induced using IPTG to a final concentration of 0.5 mM for ~12 h (overnight) at 18°C before harvesting the bacteria through centrifugation at $6000 \times g$ for 20 min at 4°C. The cell pellets were then resuspended using a lysis buffer (50 mM Tris-base, pH 7.5, 200 mM NaCl, and 5% glycerol) and lysed using sonication. The lysate was centrifuged at 13 000 rpm at 4°C, and the supernatant was passed through a 0.45-µm filter. The clarified lysate was then applied to a 5-ml MBPTrap™ HP column (Cytiva). The protein was eluted from the column isocratically with a buffer (25 mM Tris-base, pH 7.5, 200 mM NaCl, 5% glycerol, 1 mM Tris(2-carboxyethyl)phosphine (TCEP), and 10 mM maltose monohydrate) after washing the column with 5 column volumes of the lysis buffer. The protein was subsequently applied to a 5-ml HiTrap™ Heparin HP column (Cytiva) and eluted using a percentage gradient of a buffer containing 40 mM Tris-base (pH 7.5), 2 M NaCl, and 5 mM TCEP. The eluted fractions were collected and further purified using sizeexclusion chromatography with a HiLoad® 26/60 Superdex® 75 pg column (Cytiva) and a buffer composed of 20 mM Trisbase (pH 7.5), 140 mM KCl, 5 mM TCEP, and 1 mM MgCl₂. The single-peak protein fractions were pooled, concentrated using Amicon centrifugal filters (molecular weight cutoff 10 kDa, Millipore Sigma), and stored at -80° C.

Fab expression and purification

The Fab BL3-6 expression plasmid was a kind gift from Joseph Piccirilli, the University of Chicago. The Fab was expressed and purified according to published protocols [43–45]. See the supporting information for further details.

Native gel electrophoresis assay

About 200 ng of RNA was refolded and then incubated for 30 min at room temperature with different Fab or Rev protein equivalents. The gels were stained with ethidium bromide and imaged using the Azure 200 gel documentation system (Azure Biosystems). See the Supplementary data for further details.

Crystallization

The RNA sample (\sim 600 µg) was refolded in a refolding buffer containing 10 mM Tris–HCl (pH 7.5), 5 mM MgCl₂, and 300 mM NaCl as described earlier for the native gel electrophoresis assay. The refolded RNA was then incubated for 30 min at room temperature with 1.1 equivalents of the Fab and concentrated to 6 mg/ml using a 10-kDa cutoff, Amicon Ultra-1 column (Millipore Sigma). Then, Fab–RNA complexes

were passed through 0.2-um cutoff Millipore centrifugal filter units (www.emdmillipore.com). The Xtal3 Mosquito liquidhandling robot (TTP Labtech, ttplabtech.com) was used to set up sitting-drop vapor-diffusion crystallization screens at room temperature (22°C) within a humidity-controlled chamber (70% humidity) using commercially available screening kits from Hampton Research. Out of 672 conditions screened for each complex, the crystal hits were observed only for the SLIIc; SLIIcG34U; SLIIcG34C; SLIIcA31C; SLIIcG39C; SLI-IcA31C, G39C; SLIIcU14 insertion, and SLIIcA36U mutants in complex with the Fab BL3-6. However, SLIIcA36U-Fab, SLIIcG39C-Fab, and SLIIcU14 insertion-Fab complex crystals did not diffract to a high enough resolution to advance further to the structure-solving process. The best diffracting crystals for all complexes were observed within a week under several conditions. Drops containing suitable crystals were brought up to 40% glycerol for cryoprotection without changing the other compositions. The crystals were immediately flash-frozen in liquid nitrogen after being fished from the drops into the loops and transported to the Brookhaven National Laboratory (BNL) for X-ray diffraction screening and data collection.

Crystallographic data collection, processing, and analysis

The X-ray diffraction datasets were collected at the Brookhaven National Laboratory, NSLSII beamlines 17-ID-1 (AMX) and 17-ID-2 (FMX). Datasets were collected for several single crystals; however, the crystal grown in a condition with 0.2 M sodium acetate trihydrate, pH 7.0, with 20% PEG 3350 provided the best resolution of 2.42 Å for the SLIIc-Fab complex. The best diffracting crystal (3.0 Å resolution) for the SLIIcG34U-Fab complex was obtained in a condition with 0.2 M NaCl, 0.1 M Tris (pH 8.0), 12.5% polyvinylpyrrolidone, and 10% PEG 4000. Likewise, the best diffracting crystals for the SLIIcG34C-Fab complex (3.0 Å resolution), SLIIcA31C-Fab complex (3.10 Å resolution), and SLIIcA31C, G39C-Fab complex (2.75 Å resolution) were obtained in 0.02 M citric acid, 0.08 M Bis-Tris propane (pH 8.8), 16% (w/v) polyethylene glycol 3350, and 0.03% ethanol; 0.2 M ammonium nitrate, and 20% (w/v) polyethylene glycol 3350 (pH 6.2); and 0.2 M ammonium citrate dibasic and 20% (w/v) polyethylene glycol 3350 (pH 5.1), respectively. All the datasets were then integrated and scaled using the beamline on-site automated programs (AutoProc). Some datasets were also processed and analyzed using the Xia2/Dials platform on CCP4 [46, 47]. The crystallographic data suggested that the SLIIc-Fab complex was crystallized in the P1 space group and contained two complexes within the crystallographic asymmetric unit $(a = 72.36 \text{ Å}, b = 76.24 \text{ Å}, c = 82.60 \text{ Å}, \alpha = 116.56^{\circ}, \beta =$ 94.91°, and $\gamma = 102.75^{\circ}$) with the 55.72% solvent content (see Supplementary Table S2 for details of the data collection statistics). Unlike the SLIIc-Fab complex, the SLIIcG34U-Fab complex crystallized in the I222 space group, and it contained a single complex within the crystallographic asymmetric unit $(a = 90.88 \text{ Å}, b = 105.01 \text{ Å}, c = 186.60 \text{ Å}, \alpha = 90^{\circ},$ $\beta = 90^{\circ}$, and $\gamma = 90^{\circ}$). Similarly, the SLIIcA31C-Fab complex was crystallized in the P1 space group. contained two complexes within the crystallographic asymmetric unit (a = 72.87 Å, b = 75.87Å, c = 83.51 Å, $\alpha = 63.17^{\circ}$, $\beta = 71.85^{\circ}$, and γ

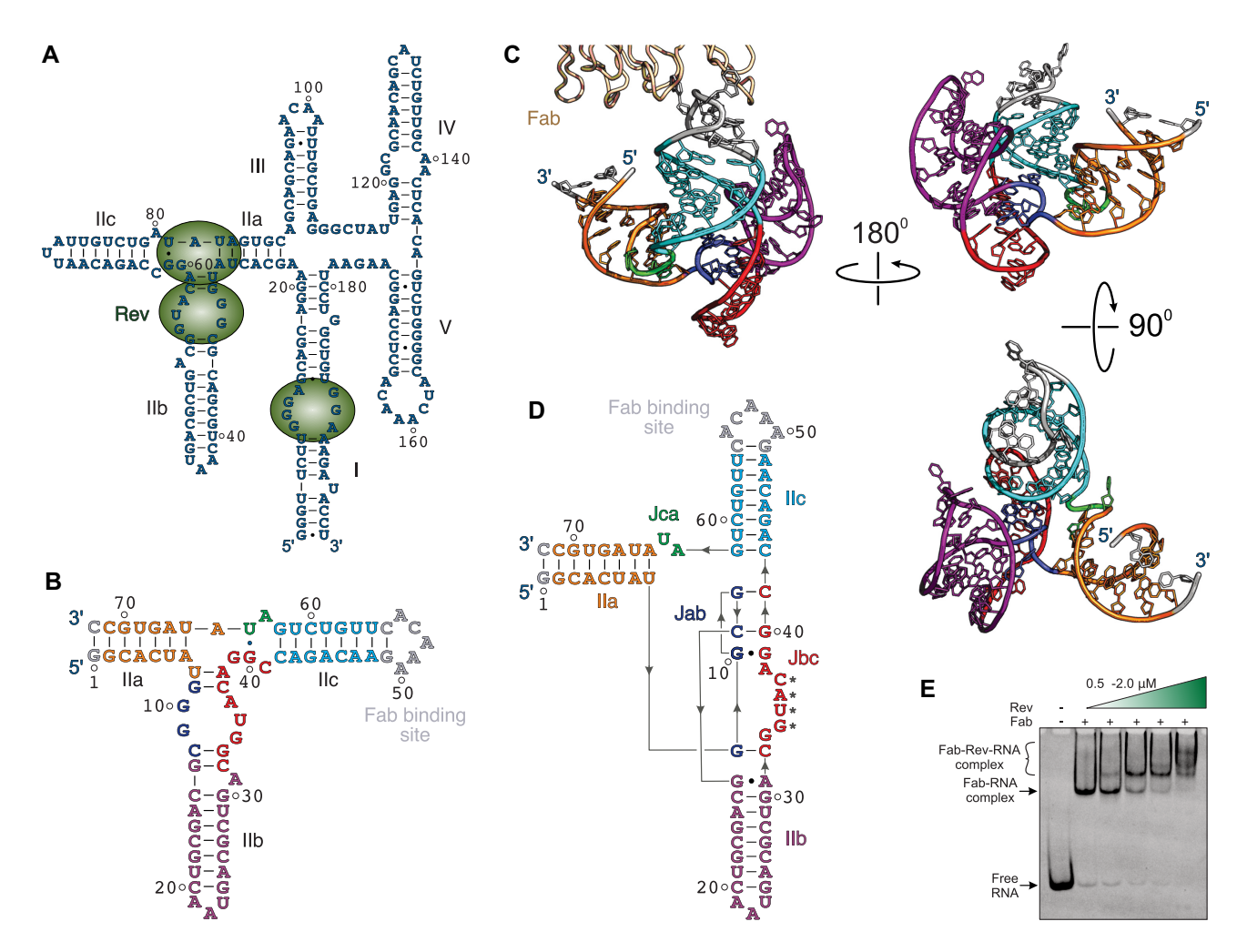


Figure 1. The overall structure of HIV-1 RRE SLII crystallized with a Fab chaperone. (**A**) A secondary structural model of a minimal HIV-1 RRE with five SL structures. The green spheres represent the Rev molecules at the previously identified high-affinity binding sites. (**B**) A secondary structure model of the SLII crystallization construct (SLIIc) in which the Fab BL3-6 binding epitope GAAACAC sequence replaces the IIc loop. The gray nucleotides indicate the mutations or insertions compared to the SLII wild-type sequence. (**C**) The crystal structure of the SLIIc cocrystallized with the Fab and determined at 2.42 Å resolution, and (**D**) its crystal-derived secondary structure. For clarity, the Fab is omitted in the rotated views. The asterisks in panel (**D**) depict the nucleotides involved in crystal contacts. (**E**) A native polyacrylamide gel showing the binding of the Fab with the crystallization construct without perturbing the Rev binding. The green color-gradient triangle shows the Rev concentration ranging from 0.5 to 2.0 μM with a 0.5 μM increment in each lane. All figure panels and corresponding labels, if any, are colored analogously for facile comparison.

= 77.75°). The SLIIcA31C, G39C–Fab complex was crystallized in the P1 space group and contained four complexes within the crystallographic asymmetric unit (a = 84.37 Å, b = 95.64 Å, c = 111.24 Å, $\alpha = 77.486^{\circ}$, $\beta = 76.34^{\circ}$, and $\gamma = 74.25^{\circ}$). The SLIIcG34C–Fab complex crystallized in the I222 space group, and it contained a single complex within the crystallographic asymmetric unit (a = 90.78 Å, b = 106.63 Å, c = 187.33 Å, $\alpha = 90^{\circ}$, $\beta = 90^{\circ}$, and $\gamma = 90^{\circ}$). Details of data collection statistics are provided in Supplementary Table S2.

For solving both structures, the initial phases were obtained by molecular replacement with the previously reported structure of Fab BL3-6 (PDB code: 8T29) [42] as the search model using Phaser on Phenix [48]. Iterative model building and refinement were performed using the COOT [49] and the Phenix package [48]. The RNA structure was built unambiguously by modeling the individual nucleotides into the electron density map obtained from the molecular replacement. The refinement used default NCS options and auto-selected TLS parameters in Phenix. The structure-

related figures were made in PyMOL (The PyMOL Molecular Graphics System, Version 2.0, Schrödinger, LLC), and the figure labels were edited in CorelDRAW (Corel Corporation, http://www.corel.com).

EM data collection, processing, and analysis

Samples for negative stain were prepared as previously described (Ohi: PMC389902) [50]. The SLIIc–Fab complex sample from the crystallographic experiments was serially diluted in the corresponding buffer (10 mM Tris–HCl, pH 7.5, 5 mM MgCl₂, and 300 mM NaCl). Formvar (10 nm)/carbon (1 nm)-coated copper grids with 400 mesh size (EMS FCF400-Cu-50) were glow-discharged for 30 s with a 5 mA current. 3.5 μl of the sample was applied to the grid and incubated for 1 min. The grid was washed twice using two drops of water and then two drops of 0.75% uranyl formate. The grids were screened for ideal concentration on a Thermo Fisher Morgagni 100 kV TEM with a Gatan Orius SC200 CCD Detector at 22 000 times magnification. A 1.2 mg/ml stock

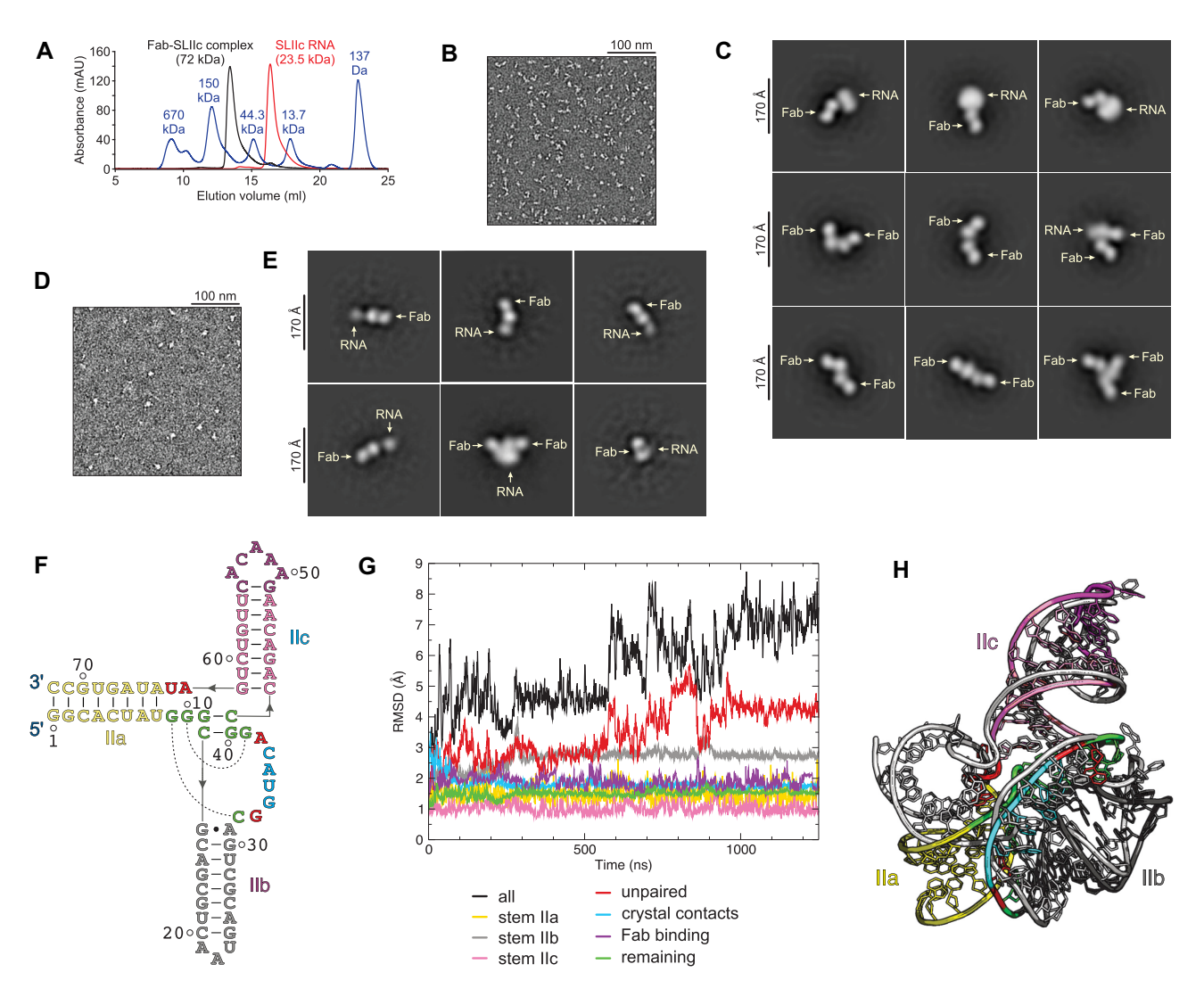


Figure 2. Size-exclusion chromatography, negative-staining EM, and MD simulation studies of the HIV-1 RRE SLII. (**A**) Representative chromatograms for the SLIIc (red), Fab–SLIIc complex (black), and a molecular size marker (blue) suggest no dimerization of the SLIIc or its Fab complex. (**B**) Representative negatively stained image of the Fab–SLIIc complex particles at a 1.2 μ g/ml concentration. (**C**) Representative 2D averages for this concentrated sample show monomers, dimers, and trimers of the Fab–SLIIc complex. The oligomerization of the complexes at this concentration is not homogeneous. (**D**) Representative negatively stained image of the same sample at a 0.24 μ g/ml concentration. (**E**) Representative 2D averages showing the Fab–SLIIc monomers in the dilute solution. The sample at a more dilute concentration is predominantly monomeric. (**F**) The crystal-derived secondary structure for the MD simulation. The stems IIa–c are colored yellow, gray, and pink, respectively. The unpaired nucleotides are colored red, and the nucleotides taking part in crystal contact are colored cyan. The nucleotides that are sequentially not part of the stem but are structurally stacked on the stems are colored green, and the nucleotides involved in the Fab binding are colored purple. The dotted curves represent long-range base-pairing interactions. (**G**) RMSDs of different structural components compared to the starting structure. Along the 1.25 μ s (1250 ns) trajectory, frames were collected every 10 ps, and RMSDs were plotted as running averages over 100 frames (1 ns). (**H**) The superposition of the final simulated structure [colored according to the secondary structure as shown in panel (F)] with the crystal structure (gray).

of the SLIIc–Fab complex was diluted 1:1000 and 1:5000 in sample buffer and imaged for data processing on a Thermo Fisher Tecnai T12 with Gatan Rio9 CMOS Detector at 36 000 times magnification, corresponding to a size of 2.08 Å per pixel, which was used for square targeting and data collection. Micrographs were collected on T12 using SerialEM [51], imported into, and processed in cryoSPARC (v4.5.1) (PMID: 28165473) [52]. CTF estimation was performed with CTFFIND4 [53]. Particle picking was performed with cryOLO v1.9.6 using a general negative stain model [54]. The box size was 200 pixels (i.e. 416 Å). About 800 357 particles for the 1:1000 dilution data set were subjected to two rounds of 2D classification, designating 100 and 50 classes. About 96 912 particles for the 1:5000 dilution data set were

subjected to one round of 2D classification, designating the 50 classes.

Molecular dynamics simulation

The MD simulations were conducted, departing from the crystal structure of the SLIIc construct. For the A63G system, guanine was modeled onto the adenine at position 63 of the SLIIc crystal structure. All MD simulations were carried out using AMBER22 [55]. The systems were neutralized with Na⁺, and additional ions were added to reach a bulk concentration of 0.14 M NaCl in a truncated octahedron box with 88 Å real-space lattice vector lengths. The systems were built with the ff99OL3 RNA [56] force field, TIP4P/Ew water model

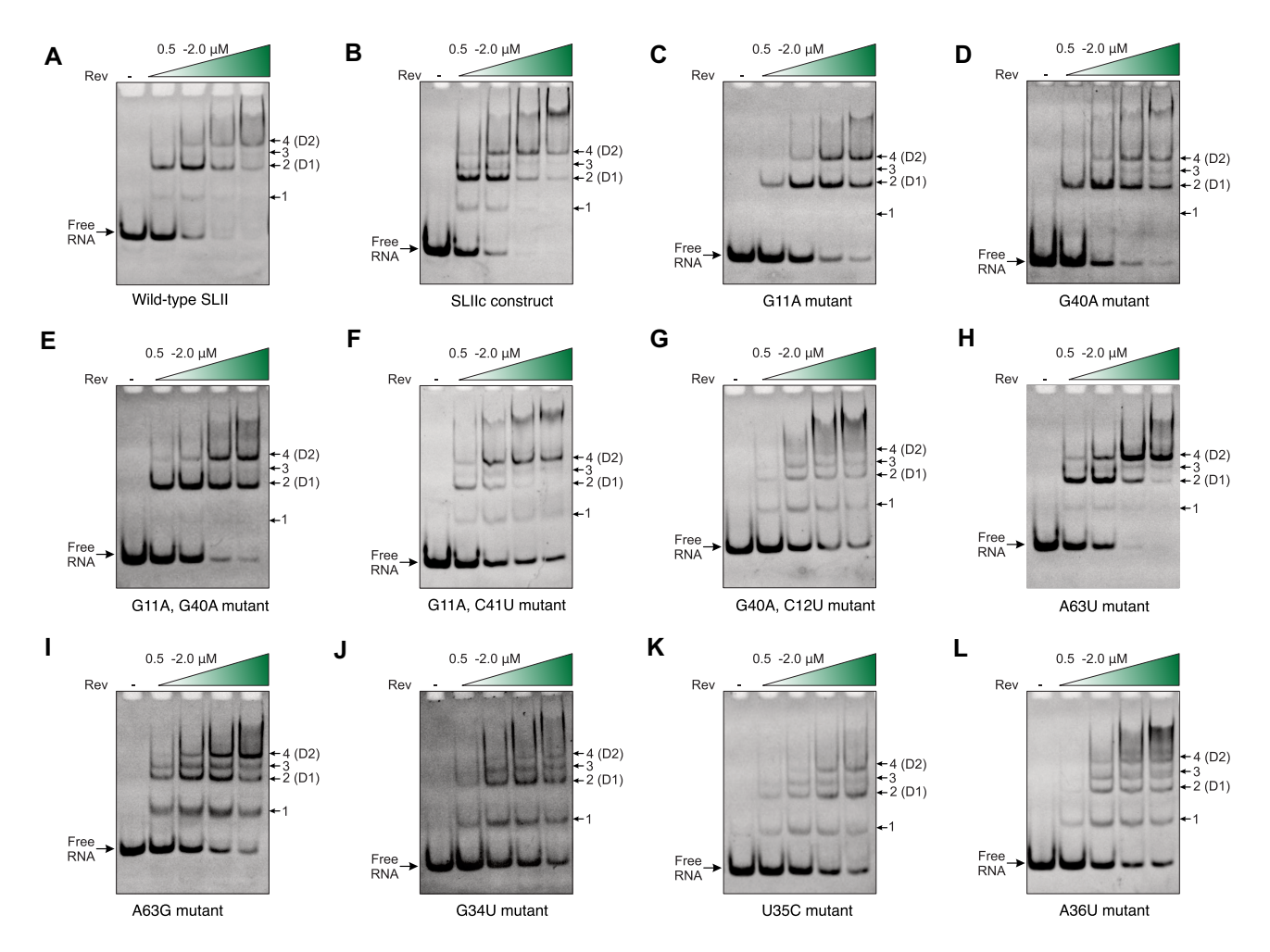


Figure 3. Binding and oligomerization of the HIV-1 Rev within the SLII 3WJ. Native polyacrylamide gels showing the Rev binding and oligomerization with the (A) wild-type SLII and (B) crystallization construct (SLIIc). Similar native gels for Rev binding with (C) G11A; (D) G40A; (E) G11A, G40A; (F) G11A, C41U; (G) G40A, C12U; (H) A63U; (I) A63G; (J) G34U; (K) U35C; and (L) A36U mutant SLIIc constructs. The green color-gradient triangle shows Rev concentration ranging from 0.5 to 2.0 μM with a 0.5 μM increment in each lane. Notably, the slowest migrating band in the presence of Rev in all gels possibly indicates higher-order complexes that have not been considered for our analysis.

[57], and corresponding Na⁺ and Cl⁻ ion parameters [58]. It should be noted that other promising and more recent force fields exist and have recently been compared [59], in particular the RNA force field developed by the Shaw group [60], the HB-CUFIX force field for helix-junction-helix (HJH) models [61], and force fields that employ CMAP corrections [62]. Here, we used the ff99OL3 force field due to its extensive validation across a wide range of RNA systems, including SLs and hairpins [63], as seen in this system, and to facilitate direct comparisons with our recent work on other RNA structures [64-68]. The simulations were then performed under periodic boundary conditions at 298 K, using a 12 Å nonbonded cutoff and PME electrostatics [64, 65]. The Langevin thermostat with $\gamma = 5 \text{ ps}^{-1}$ and the Berendsen isotropic barostat with $\tau = 1$ ps were used to maintain constant pressure and temperature. A 1 fs time step was used along with the SHAKE algorithm to fix hydrogen bond lengths [69], with three-point SHAKE for the water molecules [70]. As reported, the simulation boxes were equilibrated stepwise [71], yielding \sim 50 ns of simulation time. All simulations were carried out in constant pressure and temperature (NPT) ensembles, and 1250 ns of aggregate production was achieved per system. Root mean square deviations (RMSDs) and fluctuations (RMSFs) were calculated to quantify the structural changes and identify regions of dynamical mobility, respectively, throughout the simulation, using the starting structures as the reference.

Cellular Rev activity measurements

The HIV-1NL4-3 ΔEnv, HIV-1NL4-3 ΔRevΔEnv, HIV-1NL4-3 ΔRevΔEnvΔRRE, pcRev, and pVSV-G have been described previously [72–74]. Point mutations (A31C; G34C; G39C; A31C, G39C) and the insertion of U at position 14 in RRE SLII were made to the corresponding residues of HIV-1NL4-3 ΔRevΔEnv through overlap extension PCR, using 5′ and 3′ oligonucleotides flanking unique NheI and XhoI restriction sites in combination with oligonucleotides containing the point mutations or insertion. About 150 000 HEK 293T cells were co-transfected with 500 ng HIV-1NL4-3 ΔEnv, HIV-1NL4-3 ΔRevΔEnv, HIV-1NL4-3 ΔRevΔEnvΔRRE, or the point mutants of RRE as indicated, 50 ng of pVSV-G, and varying amounts of pcRev (0, 5, or 50 ng) using 1 mg/ml polyethyleneimine with a DNA:PEI ratio of 1:4. See the supporting information for details.

Results

SLII crystals with a Fab chaperone diffracted to 2.42 Å resolution

Our crystallization constructs span 68 nucleotides (A22 to A89) of the HIV-1 RRE that cover the intact 3WJ region of the SLII (Fig. 1A). These constructs include A22G and A89C mutations that install a G-C pair to close the IIa stem for efficient transcription and stability. Crystallization of the wild-type construct (SLII_{WT}) was unsuccessful, so we turned our efforts to Fab-assisted RNA crystallography [42, 75-77]. We prepared two crystallization constructs, SLIIb (Supplementary Fig. S1) and SLIIc (Fig. 1B), by replacing the IIb and IIc loops with the Fab BL3-6 binding hairpin-loop sequence 5' gAAACAc. The native polyacrylamide gel electrophoresis (nPAGE) assay showed that a recombinantly expressed Rev (see the "Materials and methods" section) binds to both crystallization constructs similarly compared to the SLII_{WT} construct (Fig. 3 and Supplementary Fig. S2), suggesting that the engineered Fab-binding sequence did not influence the overall folding of the SLII RNA. More importantly, the Rev also binds to these constructs in the presence of the Fab BL3-6, forming a ternary complex (Fig. 1E and Supplementary Fig. S2), supporting that the Fab binding site in these constructs is away from the Rev binding site. Thus, the Fab binding is less likely to alter the overall folding of the SLII crystallization constructs. Following the Fab and Rev binding tests, we set up the crystallization trials of both SLIIb and SLIIc constructs in complex with the Fab. However, only the SLIIc-Fab complex yielded robust crystals that diffracted to 2.42 Å resolution. The crystallographic data suggested that the SLIIc-Fab complex was crystallized in the P1 space group and contained two complexes within the crystallographic asymmetric unit (Supplementary Table S2 details the data collection statistics). The initial phases for solving the structure were obtained via molecular replacement using a previous crystal structure of Fab BL3-6 (PDB: 8T29) [42] as a search model that provided a robust electron density map, allowing the modeling of the SLII nucleotides unambiguously. After iterative rounds of model building and refinements, the final structure was determined at 2.42 Å resolution, which converged with R_{work} and R_{free} values of 20.5% and 26.5%, respectively (Supplementary Table S2 details the refinement statistics). The two SLIIc RNA copies within the crystallographic asymmetric unit appear very similar (all atoms alignment RMSD = 2.55 Å) except for some deviations in the relative orientation of the IIb helix (Supplementary Fig. S3), perhaps due to the high flexibility and dynamicity of this region, which is consistent with relatively weaker electron density map and high crystallographic B-factors observed for this region (Supplementary Fig. S4).

HIV-1 RRE SLII adopts an intricate 3WJ fold

The SLII crystal structure adopted roughly a Y-shaped topology, in which the base stem IIa bifurcates into the IIb and IIc stems to organize a 3WJ fold (Fig. 1C and Supplementary Figs S3 and S4). The IIa stem resides almost perpendicular to the IIc stem, and IIb protrudes from the IIa–IIc junction, leaning toward the IIc with the IIb loop near the 3WJ region. As shown in the crystal-derived secondary structure (Fig. 1D), starting from the 5' end, the nucleotides G1–U8 base pair with C72–A65 to form the IIa stem, and G9–C12 compose the junction (Jab) between IIa and IIb. The base pairing of G13–C20 with

G24–A31, including a noncanonical G13·A31 pair bordering the 3WJ, forms the stem IIb, which is capped by the trinucleotide A21A22U23 loop. The sequence C32–C41 comprises the IIb–IIc junction (Jbc) interacting with the Jab nucleotides via canonical and noncanonical base pairing. Following the Jbc, the C42–G49 base pairs with the C55–G62 to form the IIc stem, which is capped by the Fab binding loop used for the crystallization. Finally, the junction Jca connects the IIc and IIa helices and contains two unpaired nucleotides (A63 and U64).

The 3WI in the SLIIc crystal structure appeared complicated but well structured, with extensive interactions between the junction nucleotides, suggesting a prominent role of this junction for Rev interactions (see Supplementary Fig. S5 for details). The four nucleotides within the Jab form a sharp turn in the helix, allowing the G9 to base pair with the Jbc C32 and G10, G11, and C12 to base pair with the Jbc G39, C41, and G40, respectively. Including the G10-G39 noncanonical pair, this three-base-paired helix remains co-axially stacked with the IIc, forming almost a continuous A-form helical stem. Whereas the A38, G39, G33, and C32 remain helically stacked near the IIb and IIc stems, respectively, the nucleotides G34 to C37 flip out and form base pairs with the palindromic sequence of the symmetry-related molecule (Supplementary Fig. S6). Besides stacking interactions, the unpaired nucleotides G33 and A38 are also stabilized by hydrogen bonding interactions. The 3WJ junction connects with the stem IIb via the G13·A31 noncanonical pair, which stacks coaxially on the G9 and C32 pair. Within the Jca, the A63 and U64 nucleotides are unpaired, where U64 flips out, and A63 is stabilized through stacking interactions with the U8 and A65 base pair within the IIa stem. While the Jca nucleotides are not engaged in interactions with other junction nucleotides, the asymmetric number of the junction nucleotides (Jbc > Jab > Jca) and extensive interactions between the Jab and Jbc nucleotides define the relative positioning of the helices flanking the 3WJ. Overall, unlike a relatively simple 3WI with several noncanonical pairs as predicted based on the NMR and crystal structures of the IIb constructs [37, 38], the 3WJ in our crystal structure is stabilized by networks of base-stacking and hydrogen bonding interactions with canonical base pairs, resulting in a more extensive and well-organized junction in the context of the fulllength SLII. However, these unpaired nucleotides underscore the high dynamicity and propensity of the 3WI to adopt multiple conformations.

EM and MD simulations provide evidence of the SLII crystal structure in solution

The structural features around the 3WJ do not involve any interactions with the Fab in the crystal lattice, and Fab did not inhibit Rev binding (Fig. 1E), indicating that the overall folding of our crystal structure is unlikely to be affected by complex formation with the Fab. Additionally, while the tertiary structure of the 3WJ fold appears complicated, the base-paired nucleotides of the IIa, IIb, and IIc helices and the formation of IIb and IIc loops are consistent with previous biochemical, enzymatic probing, and SHAPE-based studies (see Supplementary Fig. S7) in the context of the full-length HIV-1 RRE or the complete HIV-1 genome [2, 31, 32, 78]. Nevertheless, the four nucleotides, G34–C37, which comprise the putative Rev binding site, were observed to form base-pairing crystal contacts with the identical nucleotides

of the symmetry-related SLIIc molecules (Supplementary Fig. S6). Therefore, we performed several experiments to determine whether these interactions exist in solution. First, sizeexclusion chromatography (SEC) analyses of the SLIIc and Fab-SLIIc complex showed single homogeneous peaks within the expected monomeric sizes compared to a standard marker, indicating that the crystallized construct does not dimerize in solution (Fig. 2A). Second, we performed negative-stain EM analysis with concentrated and dilute Fab-RNA samples. While the classification of particles isolated from images of negatively stained particles in concentrated solution showed 2D classes of what appear to be the Fab–RNA complexes as monomers, heterogeneous dimers, and trimers (Fig. 2B and C, and Supplementary Fig. S8), the 2D averages generated from particles isolated from images of negatively stained particles in the more dilute sample showed that almost all the classes were single Fab-RNA complexes, with only a few classes that appeared to be dimerized complexes (Fig. 2D and E, and Supplementary Fig. S9), showing that although Fab-RNA complexes can form heterogeneous dimers and trimers in concentrated solutions, they exist as monomers in dilute solutions. Although low resolution, none of these classes match the topology of the dimer observed in the crystal lattice (Supplementary Fig. S6), further suggesting that the base pairing of the G34-C37 nucleotides represents crystallographic contacts, and these interactions are likely irrelevant in solution. Third, we performed MD simulations using AMBER22 [55]. We examined the dynamic behavior of nucleotides in crystal contacts compared to those in the stems using MD simulations, departing from the crystal structure and monitoring the RMSDs and RMSFs (Fig. 2F-G, Figs. S10 and S11, and Supplementary Movie M1). The RMSD analyses indicated significant mobility of the relative orientations of stems IIa, IIb, and IIc rather than fluctuations occurring internally to these stems (Fig. 2G and Supplementary Fig. S10). The elevated flexibility of these regions is further highlighted in the RMSF plot (Supplementary Fig. S10), where the tail ends of stem IIa, the loop of stem IIb, and the Fab binding site in stem IIc have greater RMSF values. While crystal contact forming nucleotides (G34–C37) displayed converged RMSD values overlapping in magnitude with that of the fully base-paired stem IIa and lower RMSF values, unpaired nucleotides such as U64 showed an elevated RMSF value, indicating greater dynamical variation. Other unpaired nucleotides (G33, A38, A63, U64) exhibited high RMSD fluctuations correlating with the overall RMSD values, suggesting that internal structure of the stems, crystal contacts, and the Fab binding site are stable and remain close to the crystal structure during simulations, and thus the crystal structure represents at least a metastable free energy basin in solution (Fig. 2G and H). Notably, the four crystal-contact-forming nucleotides in the simulated structure turned toward the RNA and formed noncanonical hydrogen bonds with nearby nucleotides—specifically, C37:O2 with A38:N6, A36:N6 with O2' of G9 and C14, and G34:N7 with G9:N2 (Supplementary Fig. S10). Surprisingly, the RMSD fluctuations for the G34–C37 and unpaired nucleotide group (G33, A38, G63, U64) exhibited different behaviors in the A63G mutant SLII simulations. Although this nucleotide is located far from the crystal contacts, this behavior is likely due to sampling slightly different basins or local rearrangements in the base-pairing patterns resulting from the mutation (Supplementary Figs. S10 and S11).

3WJ comprises Rev binding and oligomerization sites

To understand the nature of SLII-Rev interactions, we performed binding studies with the SLIIc and mutant SLIIc constructs using nPAGE assays. We used a Rev construct with L12S and L60R mutations, which were shown to limit the Rev protein to dimerization [79]. We also introduced two additional mutations, P28A and V16D, to this construct and included an N-terminal MBP1 tag to enhance Rev protein solubility. First, the binding assays suggested that SLII (SLIIWT and SLIIc) binds at least four copies of the Rev molecules, as indicated by four distinct Rev–SLII complex bands, and the nature of these bands implied that SLII has two different sites for Rev dimerization (Fig. 3A and B). Whereas the Rev binding to the comparatively higher-affinity site at lower Rev concentrations likely formed a homodimeric complex with SLII (D1), the higher Rev concentrations enabled the second Rev homodimer to bind the relatively lower-affinity site (D2). Next, we introduced a series of rationally designed, base-pairing disruptive or compensatory mutations within the 3WI based on the SLIIc crystal structure and determined their Rev binding properties. Whereas G11A or G40A mutations expected to disrupt the central G40:C12 or C41:G11 pairs had a minimal effect on overall binding (based on the band intensities for free RNA), the extent of Rev binding to one of the two dimerization sites seemed to be compromised, as the Rev binding and dimerization was more limited presumably to the D1 site even at higher Rev concentrations (Fig. 3C and D). The G11A and G40A double mutation exhibited similar Rev binding patterns (Fig. 3E), indicating that these nucleotides might have important roles in regulating the Rev binding and oligomerization within the 3WJ. Nonetheless, it is possible that these mutations disrupt the D1 site, and the complex formed by Rev binding at the D2 site migrates in the gel similarly to a complex formed at the D1 site. Consistently, the base pair compensatory mutations G11A and C41U to replace the G11:C41 with the A11:U41 pair rescued the Rev-SLIIc binding to a similar level to that of the wild-type SLIIc (Fig. 3F), suggesting that this 3WJ stabilizing base pair is key for Rev binding and oligomerization with the SLII. Surprisingly, the compensatory G40A and C12U mutations that substitute the G40:C12 pairs with A40:U12 reduced the specific binding and dimerization of the Rev at both D1 and D2 sites (Fig. 3G). While these nucleotides play roles in defining the specificity of Rev binding, such unprecedented results for these rationally designed mutants indicate potential rearrangements of interactions among the 3WI nucleotides that retain a conformation pertinent to the Rev binding and oligomerization, consistent with the highly plastic nature of this RNA. Although these mutational effects on reduced binding and oligomerization are generally consistent with reduced Rev activity in previous in vivo measurements based on the translational repression assays [80], those assays did not explain the possible influence of SLII structural rearrangements on the observed Rev activities.

On the other hand, the A63U (Fig. 3H) and A63G (Fig. 3I) mutants within Jca showed similar Rev binding patterns as the wild-type SLIIc (Fig. 3B), suggesting that Jca is not the primary site for Rev binding and oligomerization. Notably, Jca nucleotides have no significant role in the 3WJ stabilization in the SLIIc crystal structure as they bulge out without any specific interaction with the junction nucleotides (Fig. 1C and Supplementary Fig. S5), which is consistent with no

effect of this bulge on Rev activity observed in previous in vivo studies [25, 81]. As primary Rev binding sites are located within the Jab and Jbc, next, we mutated nucleotides observed in the crystal contacts and performed Rev binding assays. The G34U, U35C, and A36U mutations all showed reduced overall binding with Rev, and complex formation was somewhat more restricted to Rev dimerization at the D1 site even at higher Rev concentrations (Fig. 3J-L, respectively), suggesting that these nucleotides might specifically interact with Rev and modulate the Rev oligomerization. While the reduced binding with these mutations correlates well with the nominal Rev activities observed in previous in vivo studies [80], given several unpaired nucleotides around the SLIIc 3WJ, a single-nucleotide mutation is less likely to solely account for such a robust loss of Rev binding and oligomerization specificity.

The SLIIG34U mutant crystal structure adopts an alternate fold

Our binding studies with SLII mutants, especially the nucleotides involved in crystal contacts, suggest their crucial roles in defining the overall conformational state of the SLII that modulates Rev binding and oligomerization. To test this hypothesis, we crystallized and solved the structure of the G34U mutant at 3.0 Å resolution using the same Fab-assisted crystallography approach (see Supplementary Fig. S12 and Supplementary Table S2 for statistics). Unlike the SLIIc-Fab complex, the crystallographic asymmetric unit contained a single Fab-RNA complex without significant RNA-RNA crystal contacts (Supplementary Fig. S13). Excitingly, the SLI-IcG34U crystal structure appeared in a distinctly different architecture than the SLIIc structure, especially around the 3WJ, revealing substantial structural changes induced by this single G34U mutation (Fig. 4A). In this mutant structure, the IIa stem resides nearly perpendicular to the IIc stem, and the IIb stem protrudes out from the IIa-IIc junction almost at the right angle (Fig. 4A and B). The crystal-derived secondary structure showed that the organization of the 3WJ is relatively simple compared to its wild-type SLIIc structure (Fig. 4C). While the paired and unpaired nucleotides within the IIa and IIc stems, along with the Jca, are similar in SLIIc and SLI-IcG34U structures, the reorganization of the base-pairing interactions between the Jab and Jbc nucleotides within the SLI-IcG34U 3WJ forms a more extended IIb stem than the SLIIc structure. Notably, the overall architecture of this extended IIb appears similar to the previously reported crystal structure of an isolated IIb construct [37]. Within the SLIIcG34U 3WJ structure, Jab (G9-C12) has no unpaired nucleotides due to the G9:C37, G10·U35, G11·U34, and C12:G33 base pairs (Supplementary Fig. S14). Unlike the G13·A31 noncanonical base pair in the SLIIc structure, this mutant structure formed the G13:C32 base pair, leaving the A31 unpaired and flipped out of the helix. Three of the four unpaired nucleotides G34– C37 in the SLIIc 3WJ are stabilized by the base pairing in the SLIIcG34U 3WJ with the formation of new unpaired nucleotides A38-C41 (Fig. 4C and Supplementary Fig. S14). It implies that Ibc G34-C37 nucleotides play crucial roles in defining the conformational state of the SLII, and the loss of Rev binding and oligomerization by the G34U mutation is most likely due to the re-registration of the G34-C37 interactions. The G11-U34 pair in the mutant structure would have been a G11·G34 noncanonical pair in its wild-type form. This change destabilizes the extended 3WJ to switch to the more compact form of the SLIIc, as a G11·G34 is expected to be thermodynamically less stable than a G11·U34 pair.

Structure-guided mutations favor alternative SLII conformations

Based on the observed tendency of the SLII to adopt multiple conformations, it is plausible to assume that these conformations coexist in solution, and Rev binding-induced structural rearrangements may modulate the fate of Rev interactions and oligomerization, thus affecting the nuclear export of HIV-1 RNAs. To test this hypothesis, we introduced mutations designed to favor either the compact conformation (like the wild-type structure) or the extended conformation (like the G34U mutant structure) of the SLII and conducted the Rev binding assays. First, we incorporated mutations designed to stabilize the compact conformation by introducing A31C and G39C mutations that convert the noncanonical purine:purine pairs G13·A31 and G10·G39 into the canonical pairs G13:C31 and G10:C39 in the compact conformation (Fig. 4D–F), without impacting the base-pairing pattern in the G34U-like extended conformation (Figs 1D and 4C). Interestingly, these mutations generally showed similar Rev binding patterns as the wild-type SLIIc (compact form) and perhaps facilitated the Rev oligomerization, suggesting that this conformational state of the SLII allows robust Rev binding and oligomerization. These results imply that G34-C37 nucleotides observed in crystal contacts constitute the Rev binding site. The compact form perhaps represents a Rev-bound state captured in the crystal due to stabilization by the crystal contacts, which is consistent with what has been referred to in previous studies as an "excited state" of the SLII that is favorable for Rev oligomerization [38]. Consistent with gel results, crystal structures of the A31C and A31C, G39C mutants (Fig. 4G and Supplementary Figs S15 and S16, and see Supplementary Table S2 for statistics) showed identical folds as the wild type, indicating that the conformational state of the SLII has a more pronounced effect on Rev binding and oligomerization than the specific nucleotide identity. Notably, one of the SLII molecules within the crystallographic asymmetric unit for the A31C, G39C double mutant had a slightly different rearrangement of the base-pairing pattern compared to the other three molecules (Fig. 4H and Supplementary Fig. S16), underscoring the high plasticity of this SLII 3WJ.

Next, we populated the extended conformation and introduced G11C, G40A, and G34C mutations that perturbed the base-pairing patterns in the compact fold without much effect on the extended fold. These mutants showed decreased Rev binding, and dimerization was mainly limited to one of the sites, presumably the D1 site (Fig. 4I and I). Such deleterious effects on Rev binding were not rescued by compact fold stabilizing of A31C and G39C mutations in the context of G34C mutation (Fig. 4K), indicating that the extended fold perhaps represents the most thermodynamically stable conformation of SLII, which is consistent with structural similarities between solution NMR [37] and crystal structures of the extended IIb [35-37]. As expected, the crystal structure of the G34C mutant exhibited an identical fold as the G34U mutant (Fig. 4L and Supplementary Fig. S17, and see Supplementary Table S2 for statistics), supporting that the G34 nucleotide is vital to switching the conformation of the SLII. Moreover, mutation

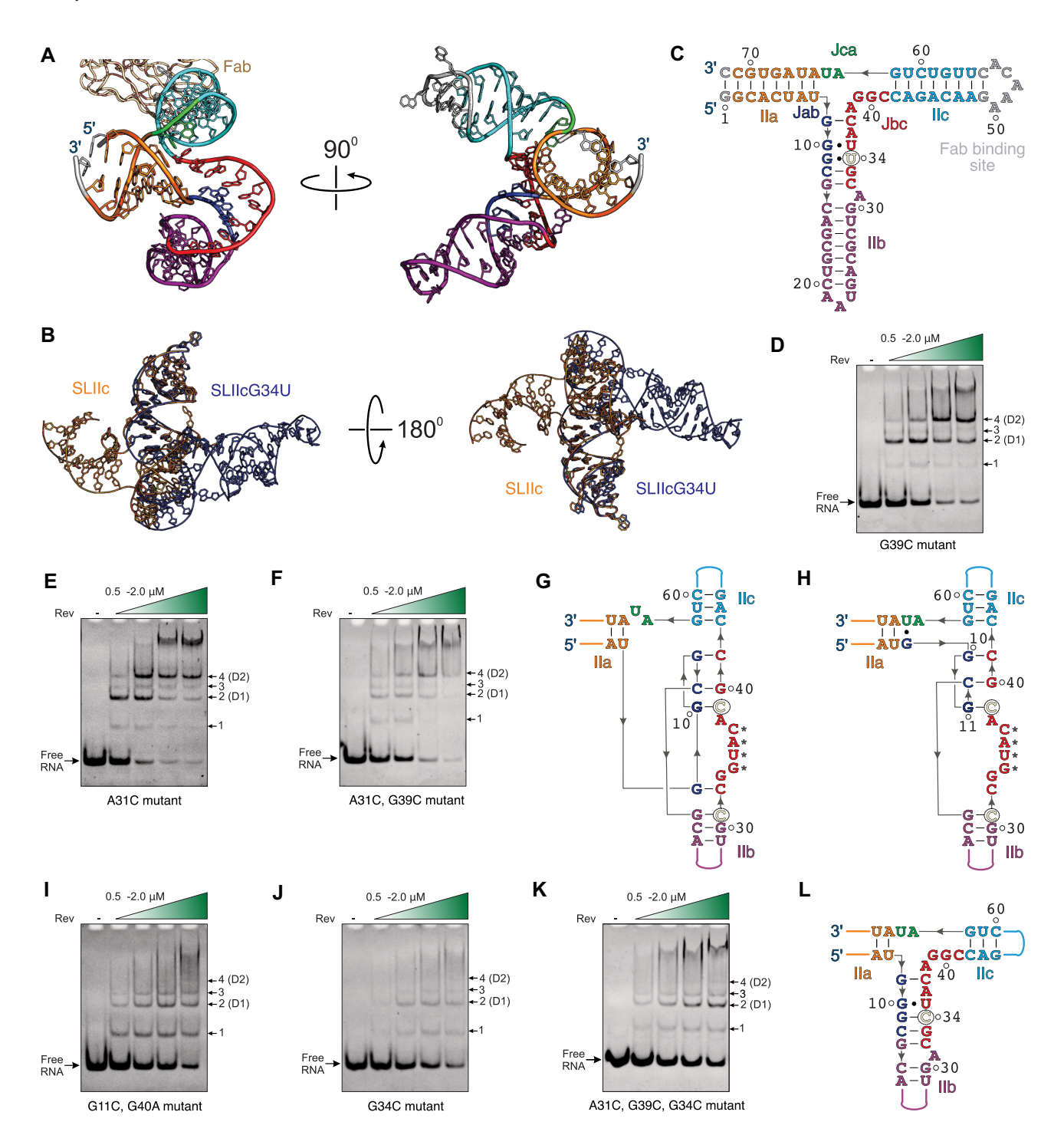


Figure 4. Crystal structures of the SLII mutants in alternative conformations. (A) The crystal structure of the G34U mutant construct cocrystallized with the Fab and determined at 3.0 Å resolution. (B) Aligning the IIc stem-loops of the SLIIc (orange) and SLIIcG34U (blue) shows relatively more compact SLIIc and extended G34U crystal structures. (C) The crystal-derived secondary structure for the G34U. For clarity, the Fab is omitted in the rotated views in panels (A) and (B). All figure panels and corresponding labels, if any, are colored analogously for facile comparison. nPAGE showing the Rev binding and oligomerization with the compact-fold-stabilizing mutants (D) G39C, (E) A31C, and (F) A31C, G39C. (G) The crystal-derived secondary structure for A31C (3.1 Å resolution) and double mutant A31C, G39C (2.75 Å resolution). (H) The structure of one of the symmetry-mates for the A31C, G39C mutant revealed a slightly different configuration of the 3WJ. nPAGE showing the Rev binding and oligomerization with the extended-fold-stabilizing mutants (I) G11C, G40A, (J) G34C, and (K) A31C, G39C, G34C. (L) The crystal-derived secondary structure for G34C (3.0 Å resolution). The green color-gradient triangle for the gels shows the Rev concentration ranging from 0.5 to 2.0 μM with a 0.5 μM increment in each lane. The mutated nucleotides are colored yellow and circled for clarity. All figure panels and corresponding labels, if any, are colored analogously for facile comparison.

of G34 to A34 to maintain the noncanonical base pairing displays a similar Rev binding pattern as the wild-type form (Fig. 5A), indicating that the purine–purine mismatch pair maintains the plasticity and dynamicity of the 3WJ structure to enable Rev binding. Additionally, the insertion of the U14 nucleotide, relatively distant from the 3WJ site, showed a similar pattern of Rev binding as the wild-type SLIIc (Fig. 5B), further supporting that the Rev binding and oligomerization occur within the 3WJ. Moreover, the binding pattern of wild-type SLIIc seems to be somewhat in between compact and extended forms, indicating that SLII can exist in multiple conformations in the solution, and structural rearrangements upon Rev binding within SLII may define the fate of the Rev binding and oligomerization.

Conformational changes correlate well with Rev activity in cells

We performed cellular assays to test how alternative folds of the SLII construct observed in crystal structures modulate the Rev activity and nuclear export of HIV-1 RNAs. In these assays, we measured Gag protein expression and infectious virion yield following transfection of HEK 293T cells with an HIV-1 ΔRev ΔEnv proviral plasmid, an Env-complementing VSV-G, and a Rev expression plasmid. The Gag expression was assessed by western blotting using HSP90 protein as a loading control. The infectious virion yield was determined by inoculating MT4 LTR-GFP indicator cells with transfected cell supernatants. Whereas A31C, G39C, and double mutant A31C, G39C behaved similarly to the wild-type construct, the Gag expression and infectious virion yield were significantly reduced for the G34C mutant (Fig. 5C and D). The U14 insertion mutant moderately reduced Gag expression and infectious virion yield (Fig. 5C and D). The lower Rev activity and nuclear export of HIV-1 RNAs, as indicated by the reduced Gag expression and infectious virion yield, are consistent with stabilizing the extended fold of the SLII as observed in our crystal structures. Notably, we observed no significant reduction in Gag expression and infectious virion yield for the compact fold-stabilizing mutants (Fig. 5C and D), suggesting that the compact crystal structure observed for the wild-type SLIIc likely represents a Rev-bound form, and the crystal contacts in the crystal lattice perhaps coincidentally stabilized such a fold. Consistent with the previous crystal structure of the IIb with a Rev dimer [37], several biochemical studies [22, 23, 31] indicated that the flexibility at the 3WJ orients the Rev molecules for adaptive recognition, binding affinity, and cooperativity. NMR studies with the isolated IIb constructs [39] also showed such flexibility in the purine-rich region of SLII. Our proposed mechanism of HIV-1 nuclear export not only explains previous observations pertinent to the RRE structure-mediated Rev binding and oligomerization, but also supports a growing view that RNAs form multiple structures that can exist as an ensemble with a dynamic equilibrium of alternative conformations with several secondary structures, modulating the biological activity [38]. For HIV-1 RRE, we propose that SLII may exist in a dynamic equilibrium of multiple conformations, toggling between the compact and extended forms, and binding the Rev shifts the equilibrium toward the compact conformations, facilitating the Rev binding and oligomerization, thus allowing robust interactions with cellular nuclear export machinery.

Discussion

Based on the observation of multiple crystal structures of the full-length SLII in two distinct conformations (see Supplementary Fig. S18 for comparisons of all structures) and Rev binding studies with the wild-type and mutant SLII constructs, we propose that the structural plasticity and conformational dynamics of the HIV-1 RRE SLII regulate Rev binding and oligomerization to define the fate of HIV-1 RNA nuclear export. As illustrated in Fig. 5E, in this model, the SLII can exist in at least two forms in solution—the compact and extended conformations. The extended conformation is consistent with previous NMR studies, and it may represent a thermodynamically more stable fold in solution in the absence of Rev. The binding of Rev to SLII thus drives the overall conformational equilibrium toward the compact form, with each subsequent Rev binding event reinforcing this shift in equilibrium toward a compact structure. Our studies suggest a model where the compact form of the SLII allows better binding and oligomerization of Rev within the HIV-1 RRE, leading to downstream interactions of the Rev-RRE complex with the host's nuclear export machinery. It is critical to note that wildtype SLII structure in solution may assume different 3WJ configurations, and mutational effects observed in our Rev binding and cellular activity measurements may be a combined effect of the disruption of specific interactions between SLII and Rev rather than the sole effect arising from toggling of RNA conformational equilibrium. However, observing multiple crystal structures for this RNA within the same crystallographic asymmetric unit and in independent crystals strongly argues that the structural plasticity of HIV-1 RRE is a significant factor in modulating Rev binding and oligomerization. Our ongoing studies of full-length RRE and RRE-Rev complex structures aim to validate these structural insights into HIV-1 RNA nuclear export mechanisms.

Notably, the mechanism of Rev-SLII interactions based on our SLII structure appears to be quite different than what was proposed based on the crystal structure of a Rev dimer in a complex with a synthetic IIb hairpin construct (PDB: 4PMI) [37]. This model predicted a series of noncanonical G·A and G·G pairs as a part of the 3WJ and stem IIb that comprised two high-affinity Rev binding and dimerization sites. However, consistent with biochemical probing and SHAPE studies [20, 24, 29–31], the nucleotides interacting with Rev are an integral part of 3WI in our structures rather than a IIb bulge, suggesting that multiple high-affinity Rev binding sites are incorporated within the SLII 3WJ. Another proposed model for RRE-Rev binding was derived from the results of a SAXSbased study by Fang et al. [39] using an intact 232-nt HIV-1 RRE construct. Starting from a SAXS-derived A-shaped structure of the RRE, this work suggests two Rev binding sites located within the SLII and SLI, separated by ~ 55 Å. As the spacing between the two RNA-binding domains in the Rev dimers resembles the spacing between these two binding sites, the authors hypothesized that initial Rev binding helps to bridge these two Rev binding sites. Although the high-resolution tertiary structure of the intact RRE has yet to be determined, our results suggest that, unlike the SAXSbased model, SLII alone can form an oligomeric RRE-Rev complex, which is also consistent with a recent native massspectrometry-based study that showed SLII can bind up to five Rev molecules [82]. Since the intact RRE has been shown to bind up to eight Rev molecules [18, 83, 84] and SLII contains

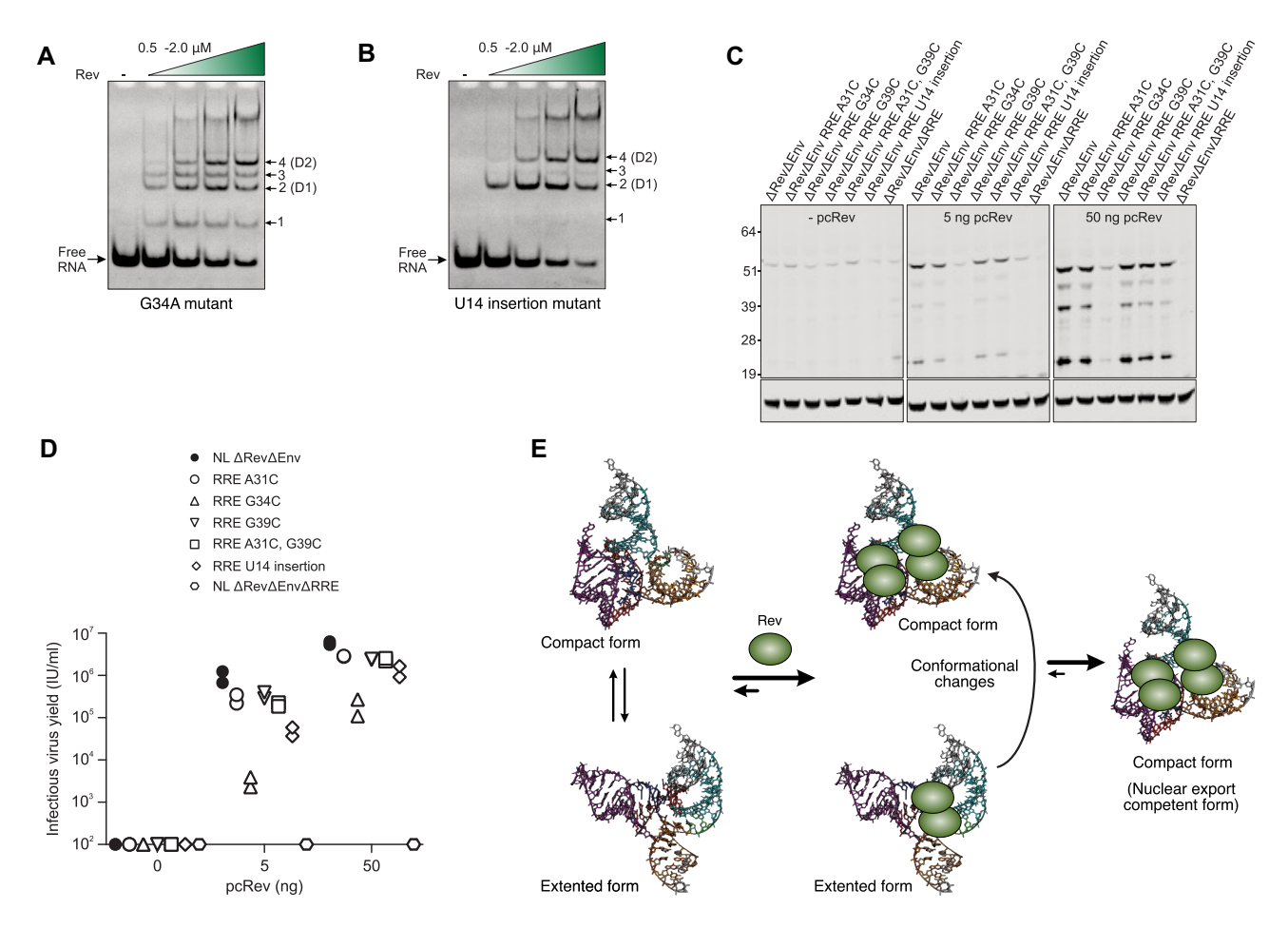


Figure 5. A structure-based model for RRE-mediated nuclear export of HIV-1 RNA. nPAGE showing the Rev binding and oligomerization with ($\bf A$) G34A mutant and ($\bf B$) U14 insertion. The green color-gradient triangle shows the Rev concentration range from 0.5 to 2.0 μM with a 0.5 μM increment in each lane. ($\bf C$) Gag expression and ($\bf D$) infectious virion yield following transfection of HEK 293T cells with HIV-1 Δ Rev Δ Env proviral plasmids, along with an Env-complementing VSV-G expression plasmid and 0, 5, or 50 ng of a Rev expression plasmid. The HIV-1 Gag expression was assessed by western blotting using an HSP90 loading control. The infectious virion yield was determined by inoculating MT4 LTR-GFP indicator cells with supernatants from transfected cells. ($\bf E$) A proposed model for Rev-RRE-mediated nuclear export of HIV-1 RNAs. The model highlights the high structural plasticity of the HIV-1 RRE SLII, which enables it to adopt multiple conformations to modulate Rev binding and oligomerization.

multiple Rev dimerization sites, SLI may serve as a secondary Rev dimerization site that facilitates the connection between SLII and SLI sites through Rev–Rev interactions. Our initial results indicate a single Rev dimer binding to an SLI construct (Supplementary Fig. S19). However, it is important to note that SLI may create an initial dimer binding site or promote the proper arrangement of the RRE–Rev oligomeric complex within the intact RRE, which warrants further investigation.

While preparing this manuscript, Tipo et al. [40] published a 2.85 Å resolution crystal structure (PDB: 8UO6) of the SLII fused with a tRNA scaffold within stem IIa [40]. While some conclusions drawn from their study, such as the location of the high-affinity Rev binding sites within the 3WJ rather than stem IIb and the presence of the higher- and lower-affinity binding sites for Rev dimerization, are consistent with our study, their SLII structure itself, especially around the 3WJ, is quite different than ours (see Supplementary Fig. S20 for detailed comparisons). Their 3WJ junction appeared extended and unstructured, with most junction nucleotides unpaired. However, our SLII crystal structures have a well-organized 3WJ with extensive canonical and noncanonical base-pairing interactions between the junction nucleotides. They proposed closed and open conformations of the SLII that differ in

reordering a single noncanonical pair observed in the two molecules within the asymmetric unit of the same crystal. However, the impact of extensive crystal contacts around the 3WI in their structures in stabilizing the open or closed conformation was unclear. The unpaired nucleotides (G34 to C37) involved in the crystal contacts in the compact form of our structures also remained unpaired in the Tipo et al. [40] structures. They match closely with our molecular dynamics results in terms of having no base-pairing interactions within the 3WI; however, unlike what is expected to be more dynamic in the Tipo et al. [40] structures (see Supplementary Fig. S20 for comparisons), these nucleotides (G34 to C37) were less dynamic than other unpaired nucleotides in MD simulations for our compact crystal structure (Fig. 2G). Nevertheless, observing these unpaired nucleotides within 3WJ in multiple crystal structures, both with and without the crystal contacts, underscores their relevance in reconfiguring the SLII conformation, thereby defining Rev binding and oligomerization in

Our G34U and G34C mutants also adopted a distinct fold compared to the conformations reported by Tipo *et al.* [40]. However, this G34U mutation appears to replace a noncanonical G10·G34 pair with a G10·U34, which would further

stabilize their "closed" form compared to the "open" conformation. These substantial differences in the 3WJ architecture extend to the overall positioning of the helices in these structures. Unlike the IIa and IIb stems, which are coaxially aligned, and the IIc, which is almost perpendicular to the IIa/IIb junction axis in Tipo et al. [40] structures, our extended conformation shows IIa and IIc stems coaxially aligned and IIb protruding out almost perpendicularly from the IIa/IIc junction axis. Regarding Rev binding, contrary to our data, which suggests that the compact SLII is more favorable for Rev interactions compared to the extended fold, Tipo et al. [40] proposed that the open conformation favors Rev binding compared to the closed form. Therefore, although SLII may exist as an ensemble of all these conformations in solution, the open and closed conformations mentioned in Tipo et al. [40] differ significantly from our extended and compact structures. For the nuclear export of HIV-1 RNAs, Rev may preferentially bind to one of the sampled SLII conformations or induce a binding-favorable conformational change within the SLII structure, which warrants further structural studies of Rev-SLII complexes. Nevertheless, these crystal structures highlight the tendency of HIV-1 RRE SLII to adopt multiple conformations, supporting a model where the structural plasticity of the RNA is an important mechanism regulating RRE-Rev interactions and function.

The nuclear export of intron-containing RNAs is essential for HIV-1 replication; therefore, the RRE-Rev platform has been an attractive therapeutic target [85, 86]. While the structures of isolated IIb have been used to direct the development of small-molecule drugs against HIV-1 infections [85, 86], our structural studies with intact SLII provide better opportunities to screen for structure-based design of inhibitors that target the well-structured, high-affinity Rev binding sites within the SLII 3WJ. Moreover, the structural plasticity of SLII observed in multiple high-resolution crystal structures would make it possible to develop small molecule drugs that selectively bind one of the conformations, especially those that significantly reduce nuclear export of HIV-1 RRE, offering various paths toward the development of anti-HIV therapeutics relative to the approaches that target a single specific conformation of the RRE.

Acknowledgements

This work was mainly supported by the Center for Structural Biology of HIV-1 RNA (CRNA) Collaborative Development Pilot Grant Program (NIH NIAID1U54AI170660, Sub-award SUBK00019302) to D.K. and partly by the NIH T32 grant (GM066706) to M.O. and NIH GM062248 to D.M.Y. The crystallographic data were collected at the NSLSII beamlines (17-ID-1 and 17-ID-2) in Brookhaven National Laboratory (BNL) using the beamtime obtained through NECAT BAG proposal #311950. The NIH-NIGMS primarily supports the BNL's Center for Bio-Molecular Structure (CBMS) through a Center Core P30 Grant (P30GM133893) and by the DOE Office of Biological and Environmental Research (KP1607011). The NSLS2 is the U.S. DOE Office of Science User Facility operated under Contract No. DE-SC0012704. Computational resources were provided by the Office of Advanced Research Computing (OARC) at Rutgers, The State University of New Jersey; the Advanced Cyberinfrastructure Coordination Ecosystem: Services and Support (ACCESS) program (supercomputer Expanse at SDSC through allocation

CHE190067); and the Texas Advanced Computing Center (TACC) at the University of Texas at Austin (supercomputer Frontera through allocation CHE20002). The authors also thank Prof. Michael F. Summers, University of Maryland, Baltimore County, for critical review and feedback on the initial manuscript.

Author contributions: D.K. and M.O. conceived and designed the experiments. M.O. prepared the samples, conducted most of the crystallographic and binding experiments, and solved the crystal structures with the help of D.K. L.H purified the Rev protein and helped M.O. with binding experiments under the mentorship of J.M. A.P performed and analyzed the EM work in the laboratory of M.D.O. T.Z. conducted cellular Rev activity assays in the laboratory of P.D.B. L.L and S.E. performed the molecular dynamics simulation study and analyzed the results with D.M.Y. Undergraduate researchers J.D., M.N., and H.P. assisted M.O. with biochemical experiments and crystallization trials set up. M.O. analyzed most of the biochemical and crystallographic data and interpreted the results with D.K. M.O and D.K. wrote the manuscript with support from D.M.Y., M.D.O., J.M., and P.D.B. All authors reviewed the manuscript.

Supplementary data

Supplementary data is available at NAR online.

Conflict of interest

None declared.

Funding

The Center for Structural Biology of HIV-1 RNA (CRNA) Collaborative Development Pilot Grant Program (NIH NIAID1U54AI170660-01, Sub-award SUBK00019302) and National Institute of General Medical Sciences [1R35GM150869 to D.K. and R01GM062248 to D.M.Y.]. Funding to pay the Open Access publication charges for this article was provided by National Institute of General Medical Sciences [1R35GM150869].

Data availability

The atomic coordinates and structure factors for the reported crystal structures of SLIIc; SLIIcG34U; SLIIcG34C; SLIIcA31C; and SLIIcA31C, G39C, all in complex with Fab BL3-6, have been deposited with the Protein Data Bank under accession codes 9C2K, 9C75, 9E7G, 9E7D, and 9E7E, respectively. All data are available in the main text or supplementary material. The authors will provide plasmids for the expression of Fab BL3-6 and Rev upon reasonable request. Requests should be directed to D.K.

References

- Freed EO. HIV-1 replication. Somatic Cell Mol Genet 2001;26:13–33. https://doi.org/10.1023/A:1021070512287
- Watts JM, Dang KK, Gorelick RJ et al. Architecture and secondary structure of an entire HIV-1 RNA genome. Nature 2009;460:711–6. https://doi.org/10.1038/nature08237

- Sundquist WI, Kräusslich H-G. HIV-1 assembly, budding, and maturation. Cold Spring Harb Perspect Med 2012;2:a006924. https://doi.org/10.1101/cshperspect.a006924
- Chang DD, Sharp PA. Messenger RNA transport and HIV Rev regulation. *Science* 1990;249:614–5. https://doi.org/10.1126/science.2143313
- Malim MH, Cullen BR. HIV-1 structural gene expression requires the binding of multiple rev monomers to the viral RRE: implications for HIV-1 latency. *Cell* 1991;65:241–8. https://doi.org/10.1016/0092-8674(91)90158-U
- Kjems J, Frankel AD, Sharp PA. Specific regulation of mRNA splicing *in vitro* by a peptide from HIV-1 Rev. *Cell* 1991;67:169–78. https://doi.org/10.1016/0092-8674(91)90580-R
- Malim MH, Hauber J, Le S-Y et al. The HIV-1 Rev trans-activator acts through a structured target sequence to activate nuclear export of unspliced viral mRNA. Nature 1989;338:254–7. https://doi.org/10.1038/338254a0
- 8. Chang DD, Sharp PA. Regulation by HIV Rev depends upon recognition of splice sites. *Cell* 1989;59:789–95. https://doi.org/10.1016/0092-8674(89)90602-8
- Malim MH, Tiley LS, McCarn DF et al. HIV-1 structural gene expression requires binding of the Rev trans-activator to its RNA target sequence. Cell 1990;60:675–83. https://doi.org/10.1016/0092-8674(90)90670-A
- Fornerod M, Ohno M, Yoshida M et al. CRM1 is an export receptor for leucine-rich nuclear export signals. Cell 1997;90:1051–60. https://doi.org/10.1016/S0092-8674(00)80371-2
- 11. Wolff B, Sanglier J-J, Wang Y. Leptomycin B is an inhibitor of nuclear export: inhibition of nucleo-cytoplasmic translocation of the human immunodeficiency virus type 1 (HIV-1) Rev protein and Rev-dependent mRNA. Chem Biol 1997;4:139–47.
- Cullen BR. Nuclear RNA export pathways. Mol Cell Biol 2000;20:4181–87. https://doi.org/10.1128/MCB.20.12.4181-4187.2000
- Zapp ML, Stern S, Green MR. Small molecules that selectively block RNA binding of HIV-1 Rev protein inhibit Rev function and viral production. *Cell* 1993;74:969–78. https://doi.org/10.1016/0092-8674(93)90720-B
- Ratmeyer L, Zapp ML, Green MR et al. Inhibition of HIV-1 Rev-RRE interaction by diphenylfuran derivatives. Biochemistry 1996;35:13689-96. https://doi.org/10.1021/bi960954v
- Jin Y, Cowan J. Targeted cleavage of HIV Rev response element RNA by metallopeptide complexes. J Am Chem Soc 2006;128:410–1. https://doi.org/10.1021/ja055272m
- Daugherty MD, Booth DS, Jayaraman B. et al. HIV Rev response element (RRE) directs assembly of the Rev homooligomer into discrete asymmetric complexes. Proc Natl Acad Sci USA 2010;107:12481–6. https://doi.org/10.1073/pnas.1007022107
- 17. Huang XJ, Hope TJ, Bond BL *et al.* Minimal Rev-response element for type 1 human immunodeficiency virus. *J Virol* 1991;65:2131–4. https://doi.org/10.1128/jvi.65.4.2131-2134.1991
- Cook KS, Fisk GJ, Hauber J et al. Characterization of HIV-1 REV protein: binding stoichiometry and minimal RNA substrate. Nucleic Acids Res 1991;19:1577–83. https://doi.org/10.1093/nar/19.7.1577
- 19. Heaphy S, Finch JT, Gait MJ et al. Human immunodeficiency virus type 1 regulator of virion expression, Rev, forms nucleoprotein filaments after binding to a purine-rich "bubble" located within the Rev-responsive region of viral mRNAs. Proc Natl Acad Sci USA 1991;88:7366–70. https://doi.org/10.1073/pnas.88.16.7366
- 20. Kjems J, Brown M, Chang DD *et al*. Structural analysis of the interaction between the human immunodeficiency virus Rev protein and the Rev response element. *Proc Natl Acad Sci USA* 1991;88:683–7. https://doi.org/10.1073/pnas.88.3.683
- 21. Mann DA, Mikaélian I, Zemmel RW *et al.* A molecular rheostat. Co-operative Rev binding to stem I of the Rev-response element modulates human immunodeficiency virus type-1 late gene

- expression. *J Mol Biol* 1994;241:193–207. https://doi.org/10.1006/jmbi.1994.1488
- 22. Zemmel RW, Kelley AC, Karn J *et al.* Flexible regions of RNA structure facilitate co-operative Rev assembly on the Rev-response element. *J Mol Biol* 1996;258:763–77. https://doi.org/10.1006/jmbi.1996.0285
- 23. Daugherty MD, D'Orso I, Frankel AD. A solution to limited genomic capacity: using adaptable binding surfaces to assemble the functional HIV Rev oligomer on RNA. *Mol Cell* 2008;31:824–34. https://doi.org/10.1016/j.molcel.2008.07.016
- 24. Legiewicz M, Badorrek CS, Turner KB et al. Resistance to RevM10 inhibition reflects a conformational switch in the HIV-1 Rev response element. Proc Natl Acad Sci USA 2008;105:14365–70. https://doi.org/10.1073/pnas.0804461105
- 25. Holland SM, Ahmad N, Maitra RK et al. Human immunodeficiency virus Rev protein recognizes a target sequence in Rev-responsive element RNA within the context of RNA secondary structure. J Virol 1990;64:5966–75. https://doi.org/10.1128/jvi.64.12.5966-5975.1990
- 26. Olsen HS, Cochrane AW, Dillon PJ et al. Interaction of the human immunodeficiency virus type 1 Rev protein with a structured region in env mRNA is dependent on multimer formation mediated through a basic stretch of amino acids. Genes Dev 1990;4:1357–64. https://doi.org/10.1101/gad.4.8.1357
- 27. Fenster SD, Wagner RW, Froehler BC *et al.* Inhibition of human immunodeficiency virus type-1 env expression by C-5 propyne oligonucleotides specific for Rev-response element stem-loop V. *Biochemistry* 1994;33:8391–8. https://doi.org/10.1021/bi00194a002
- 28. O'Carroll IP, Thappeta Y, Fan L *et al.* Contributions of individual domains to function of the HIV-1 Rev response element. *J Virol* 2017;91:e00746-17.
- Kjems J, Calnan BJ, Frankel AD *et al.* Specific binding of a basic peptide from HIV-1 Rev. *EMBO J* 1992;11:1119–29. https://doi.org/10.1002/j.1460-2075.1992.tb05152.x
- 30. Charpentier B, Stutz F, Rosbash M. A dynamic *in vivo* view of the HIV–IRev–RRE interaction. *J Mol Biol* 1997;266:950–62. https://doi.org/10.1006/jmbi.1996.0858
- 31. Bai Y, Tambe A, Zhou K *et al.* RNA-guided assembly of Rev–RRE nuclear export complexes. *eLife* 2014;3:e03656. https://doi.org/10.7554/eLife.03656
- 32. Sherpa C, Rausch JW, Le Grice SF *et al.* The HIV-1 Rev response element (RRE) adopts alternative conformations that promote different rates of virus replication. *Nucleic Acids Res* 2015;43:4676–86. https://doi.org/10.1093/nar/gkv313
- Battiste JL, Mao H, Rao NS et al. Alpha helix-RNA major groove recognition in an HIV-1 Rev peptide–RRE RNA complex. Science 1996;273:1547–51. https://doi.org/10.1126/science.273.5281.1547
- 34. Peterson RD, Feigon J. Structural change in Rev responsive element RNA of HIV-1 on binding Rev peptide. J Mol Biol 1996;264:863–77. https://doi.org/10.1006/jmbi.1996.0683
- Hung L-W, Holbrook EL, Holbrook SR. The crystal structure of the Rev binding element of HIV-1 reveals novel base pairing and conformational variability. *Proc Natl Acad Sci USA* 2000;97:5107–12. https://doi.org/10.1073/pnas.090588197
- 36. Ippolito JA, Steitz TA. The structure of the HIV-1 RRE high-affinity Rev binding site at 1.6 Å resolution. *J Mol Biol* 2000;295:711–7. https://doi.org/10.1006/jmbi.1999.3405
- Jayaraman B, Crosby DC, Homer C et al. RNA-directed remodeling of the HIV-1 protein Rev orchestrates assembly of the Rev–Rev response element complex. eLife 2014;3,e04120. https://doi.org/10.7554/eLife.04120
- Chu CC, Plangger R, Kreutz C et al. Dynamic ensemble of HIV-1 RRE stem IIB reveals non-native conformations that disrupt the Rev-binding site. Nucleic Acids Res 2019;47:7105–17. https://doi.org/10.1093/nar/gkz498

- Fang X, Wang J, O'Carroll IP. An unusual topological structure of the HIV-1 Rev response element. *Cell* 2013;155:594–605. https://doi.org/10.1016/j.cell.2013.10.008
- 40. Tipo J, Gottipati K, Slaton M *et al.* Structure of HIV-1 RRE stem-loop II identifies two conformational states of the high-affinity Rev binding site. *Nat Commun* 2024;15:4198. https://doi.org/10.1038/s41467-024-48162-y
- 41. Das NK, Hollmann NM, Vogt J *et al.* Crystal structure of a highly conserved enteroviral 5' cloverleaf RNA replication element. *Nat Commun* 2023;14:1955. https://doi.org/10.1038/s41467-023-37658-8
- 42. Ojha M, Vogt J, Das NK *et al.* Structure of saguaro cactus virus 3' translational enhancer mimics 5' cap for eIF4E binding. *Proc Natl Acad Sci USA* 2024;121:e2313677121. https://doi.org/10.1073/pnas.2313677121
- 43. Ye J-D, Tereshko V, Frederiksen JK et al. Synthetic antibodies for specific recognition and crystallization of structured RNA. Proc Natl Acad Sci USA 2008;105:82–7. https://doi.org/10.1073/pnas.0709082105
- 44. Koldobskaya Y, Duguid EM, Shechner DM *et al.* A portable RNA sequence whose recognition by a synthetic antibody facilitates structural determination. *Nat Struct Mol Biol* 2011;18:100–6. https://doi.org/10.1038/nsmb.1945
- 45. Paduch M, Koide A, Uysal S *et al.* Generating conformation-specific synthetic antibodies to trap proteins in selected functional states. *Methods* 2013;60:3–14. https://doi.org/10.1016/j.ymeth.2012.12.010
- Winter G, Waterman DG, Parkhurst JM. DIALS: implementation and evaluation of a new integration package. *Acta Crystallogr D Struct Biol* 2018;74:85–97. https://doi.org/10.1107/S2059798317017235
- 47. Agirre J, Atanasova M, Bagdonas H. The CCP4 suite: integrative software for macromolecular crystallography. *Acta Crystallogr D Struct Biol* 2023;79:449–61. https://doi.org/10.1107/S2059798323003595
- 48. Adams PD, Afonine PV, Bunkóczi G *et al.* PHENIX: a comprehensive Python-based system for macromolecular structure solution. *Acta Crystallogr D Biol Crystallogr* 2010;66:213–21. https://doi.org/10.1107/S0907444909052925
- 49. Emsley P, Lohkamp B, Scott WG *et al.* Features and development of Coot. *Acta Crystallogr D Biol Crystallogr* 2010;66:486–501. https://doi.org/10.1107/S0907444910007493
- 50. Ohi M, Li Y, Cheng Y *et al.* Negative staining and image classification—powerful tools in modern electron microscopy. *Biol Proced Online* 2004;6:23–34. https://doi.org/10.1251/bpo70
- Mastronarde DN. Automated electron microscope tomography using robust prediction of specimen movements. *J Struct Biol* 2005;152:36–51. https://doi.org/10.1016/j.jsb.2005.07.007
- Punjani A, Rubinstein JL, Fleet DJ et al. cryoSPARC: algorithms for rapid unsupervised cryo-EM structure determination. Nat Methods 2017;14:290–6. https://doi.org/10.1038/nmeth.4169
- Rohou A, Grigorieff N. CTFFIND4: fast and accurate defocus estimation from electron micrographs. J Struct Biol 2015;192:216–21. https://doi.org/10.1016/j.jsb.2015.08.008
- 54. Wagner T, Merino F, Stabrin M. SPHIRE-crYOLO is a fast and accurate fully automated particle picker for cryo-EM. Commun Biol 2019;2:218. https://doi.org/10.1038/s42003-019-0437-z
- 55. Case DA, Aktulga HM, Belfon K. AmberTools. *J Chem Inf Model* 2023;63:6183–91. https://doi.org/10.1021/acs.jcim.3c01153
- Pérez A, Marchán I, Svozil D et al. Refinement of the AMBER force field for nucleic acids: improving the description of alpha/gamma conformers. Biophys J 2007;92:3817–29. https://doi.org/10.1529/biophysj.106.097782
- 57. Horn HW, Swope WC, Pitera JW et al. Development of an improved four-site water model for biomolecular simulations: TIP4P-Ew. J Chem Phys 2004;120:9665–78. https://doi.org/10.1063/1.1683075
- Joung IS, Cheatham TE 3rd. Determination of alkali and halide monovalent ion parameters for use in explicitly solvated

- biomolecular simulations. *J Phys Chem B* 2008;112:9020–41. https://doi.org/10.1021/jp8001614
- Choi T, Li Z, Song G et al. Comprehensive comparison and critical assessment of RNA-specific force fields. J Chem Theory Comput 2024;20:2676–88. https://doi.org/10.1021/acs.jctc.4c00066
- 60. Tan D, Piana S, Dirks RM et al. RNA force field with accuracy comparable to state-of-the-art protein force fields. Proc Natl Acad Sci USA 2018;115:E1346–55. https://doi.org/10.1073/pnas.1713027115
- 61. He W, Naleem N, Kleiman D et al. Refining the RNA force field with small-angle X-ray scattering of helix–junction–helix RNA. J Phys Chem Lett 2022;13:3400–8. https://doi.org/10.1021/acs.jpclett.2c00359
- Chen J, Liu H, Cui X et al. RNA-specific force field optimization with CMAP and reweighting. J Chem Inf Model 2022;62:372–85. https://doi.org/10.1021/acs.jcim.1c01148
- 63. Deng N-J, Cieplak P. Free energy profile of RNA hairpins: a molecular dynamics simulation study. *Biophys J* 2010;98:627–36. https://doi.org/10.1016/j.bpj.2009.10.040
- 64. Darden T, York D, Pedersen L. Particle mesh Ewald: an $N \cdot \log(N)$ method for Ewald sums in large systems. *J Chem Phys* 1993;98:10089–92. https://doi.org/10.1063/1.464397
- 65. Essmann U, Perera L, Berkowitz M et al. A smooth particle mesh Ewald method. J Chem Phys 1995;103:8577–93. https://doi.org/10.1063/1.470117
- 66. Wilson TJ, McCarthy E, Ekesan Ş et al. The role of general acid catalysis in the mechanism of an alkyl transferase ribozyme. ACS Catal 2024;14:15294–305. https://doi.org/10.1021/acscatal.4c04571
- Weissman B, Ekesan Ş, Lin H-C et al. Dissociative transition state in hepatitis delta virus ribozyme catalysis. J Am Chem Soc 2023;145:2830–9. https://doi.org/10.1021/jacs.2c10079
- 68. Ekesan Ş, McCarthy E, Case DA *et al.* RNA electrostatics: how ribozymes engineer active sites to enable catalysis. *J Phys Chem B* 2022;126:5982–90. https://doi.org/10.1021/acs.jpcb.2c03727
- 69. Ryckaert J-P, Ciccotti G, Berendsen HJC. Numerical integration of the Cartesian equations of motion of a system with constraints: molecular dynamics of *n*-alkanes. *J Comput Phys* 1977;23:327–41. https://doi.org/10.1016/0021-9991(77)90098-5
- Miyamoto S, Kollman PA. Settle: an analytical version of the SHAKE and RATTLE algorithm for rigid water models. *J Comput Chem* 1992;13:952–62. https://doi.org/10.1002/jcc.540130805
- 71. McCarthy E, Ekesan Ş, Giese TJ *et al.* Catalytic mechanism and pH dependence of a methyltransferase ribozyme (MTR1) from computational enzymology. *Nucleic Acids Res* 2023;51:4508–18. https://doi.org/10.1093/nar/gkad260
- Malim MH, Hauber J, Fenrick R et al. Immunodeficiency virus Rev trans-activator modulates the expression of the viral regulatory genes. Nature 1988;335:181–3. https://doi.org/10.1038/335181a0
- 73. Yee J-K, Friedmann T, Burns JC. Generation of high-titer pseudotyped retroviral vectors with very broad host range. In: Roth MG (ed.), Methods in Cell Biology, Vol. 43. Oxford: Academic Press, 1994, 99–112.
- 74. Kutluay SB, Zang T, Blanco-Melo D et al. Global changes in the RNA binding specificity of HIV-1 gag regulate virion genesis. Cell 2014;159:1096–109. https://doi.org/10.1016/j.cell.2014.09.057
- Das NK, Hollmann NM, Vogt J et al. Crystal structure of a highly conserved enteroviral 5' cloverleaf RNA replication element. Nat Commun 2023;14:1955. https://doi.org/10.1038/s41467-023-37658-8
- Banna HA, Das NK, Ojha M et al. Advances in chaperone-assisted RNA crystallography using synthetic antibodies. BBA Adv 2023;4:100101. https://doi.org/10.1016/j.bbadva.2023.100101
- 77. Das NK, Vogt J, Patel A *et al.* Structural basis for a highly conserved RNA-mediated enteroviral genome replication. *Nucleic Acids Res* 2024;52:11218–33. https://doi.org/10.1093/nar/gkae627

- Siegfried NA, Busan S, Rice GM et al. RNA motif discovery by SHAPE and mutational profiling (SHAPE-MaP). Nat Methods 2014;11:959–65. https://doi.org/10.1038/nmeth.3029
- Daugherty MD, Liu B, Frankel AD. Structural basis for cooperative RNA binding and export complex assembly by HIV Rev. Nat Struct Mol Biol 2010;17:1337–42. https://doi.org/10.1038/nsmb.1902
- 80. Jain C, Belasco JG. A structural model for the HIV-1 Rev–RRE complex deduced from altered-specificity Rev variants isolated by a rapid genetic strategy. *Cell* 1996;87:115–25. https://doi.org/10.1016/S0092-8674(00)81328-8
- 81. Charpentier B, Stutz F, Rosbash M. A dynamic *in vivo* view of the HIV-I Rev–RRE interaction. *J Mol Biol* 1997;**266**:950–62. https://doi.org/10.1006/jmbi.1996.0858
- 82. Schneeberger E-M, Halper M, Palasser M. et al. Native mass spectrometry reveals the initial binding events of HIV-1 Rev to

- RRE stem II RNA. *Nat Commun* 2020;11:5750. https://doi.org/10.1038/s41467-020-19144-7
- 83. Daly TJ, Cook KS, Gray GS *et al.* Specific binding of HIV-1 recombinant Rev protein to the Rev-responsive element *in vitro*. *Nature* 1989;342:816–9. https://doi.org/10.1038/342816a0
- 84. Tiley LS, Malim MH, Tewary HK et al. Identification of a high-affinity RNA-binding site for the human immunodeficiency virus type 1 Rev protein. Proc Natl Acad Sci USA 1992;89:758–62. https://doi.org/10.1073/pnas.89.2.758
- Wynn JE, Santos WL. HIV-1 drug discovery: targeting folded RNA structures with branched peptides. Org Biomol Chem 2015;13:5848–58. https://doi.org/10.1039/C5OB00589B
- Sherpa C, Grice S. Structural fluidity of the human immunodeficiency virus Rev response element. *Viruses* 2020;12:86. https://doi.org/10.3390/v12010086